A SEARCH FOR THE REACTION

$$\mu^- + Cu \rightarrow e^+ + Co$$

by

Douglas Andrew Bryman

Thesis submitted to the Graduate Faculty of the

Virginia Polytechnic Institute and State University

in partial fulfillment of the requirements for the degree of

DOCTOR OF PHILOSOPHY

in

Physics

APPROVED:

K. Gotow, Chairman

M. Blecher

J. A. Jacobs

D. M. Kaplan

D. A. Jenkins

January, 1972

Blacksburg, Virginia

ACKNOWLEDGEMENTS

I would like to express my extreme gratitude to my advisor, Professor Kazuo Gotow, for his astute guidance and thoughtful participation in every phase of this work.

Professor Marvin Blecher deserves special appreciation for his able assistance from the inception to the conclusion of the project.

I would also like to thank Professor Richard Powers for his helpful participation in the second run of the experiment.

Professors J. A. Jacobs, D. M. Kaplan, and D. A. Jenkins read the manuscript.

Professor R. T. Siegel and the staff of the Space Radiation Effects Laboratory were helpful during the running of the experiment. Mr. M. D. Holt and the computer staff at SREL provided us with a well running data acquisition system.

Mr. Henry Whitehead constructed much of the spark chamber electronics.

This work was supported in part by the National Aeronautics and Space Administration.

TABLE OF CONTENTS

LIST OF TABLES

LIST OF FIGURES

CHAPTER I

INTRODUCTION

It has been observed for some time that the number of leptons (electrons, muons, electron neutrinos, and muon neutrinos) in any reaction is conserved.[1] This is normally expressed in terms of a conserved, additive lepton quantum number, which is assigned +1 to the electron (e^-), negative muon (μ^-), electron neutrino (ν_e), and muon neutrino (ν_μ), and -1 to their anti-particles (e^+, μ^+, $\bar{\nu}_e$, $\bar{\nu}_\mu$). All other known particles have zero lepton number.

The absence of several hypothetical leptonic and semi-leptonic reactions involving muon-electron transitions and the experimentally confirmed existence of two distinct two-component neutrinos[1] have led to the consideration of an additional quantum number which subdivides the leptons. The most commonly accepted scheme employs an additive, conserved muon number with values +1 for μ^-, ν_μ, -1 for μ^+, $\bar{\nu}_\mu$, and zero for all other particles. However, it is also possible to have a multiplicative muon quantum number with values -1 for μ^-, μ^+, ν_μ, $\bar{\nu}_\mu$ and +1 for the rest. Under either the additive or multiplicative muon number classification, the existence of two distinct two-component neutrinos is required.

Another manner of classification for the leptons[2] uses a single additive lepton number with opposite sign for e^-

and μ^-: +1 for e^-, μ^+, ν_e, $\bar{\nu}_\mu$, -1 for their anti-particles, and zero for all others. No separate muon number is needed. This scheme has the economical feature that $\bar{\nu}_\mu$ and ν_e can be described, respectively, as the negative and positive chiral projections of one four-component neutrino, i. e. $\phi_{\bar{\nu}_\mu} = [(1-\gamma_5)/2]\phi_\nu$ and $\phi_{\nu_e} = [(1+\gamma_5)/2]\phi_\nu$, where $\phi_{\bar{\nu}_\mu}$ and ϕ_{ν_e} are the two-component fields which destroy the muon anti-neutrino and the electron neutrino states, respectively, γ_5 is the product of the four Dirac matrices, $\gamma_5 = \gamma_1\gamma_2\gamma_3\gamma_4$, and ϕ_ν is the four-component neutrino field.

Assignment of different magnitudes of lepton number to the (e^-, ν_e) pair and the (μ^-, ν_μ) pair can also lead to a conservation scheme.[3]

Current experimental evidence does not admit a preference for any one of the proposed laws. They are consistent with all known processes, including muon decay,

$$\mu^+ \rightarrow e^+ + \nu_e + \bar{\nu}_\mu, \qquad (1)$$

and ordinary muon capture,

$$\mu^- + (Z, A) \rightarrow \nu_\mu + (Z-1, A), \qquad (2)$$

where (Z, A) refers to a nucleus with Z protons and A-Z neutrons. None allows the hypothetical, and as yet unobserved, reactions

$$\mu^+ \rightarrow e^+ + \gamma, \qquad (3)$$

$$\mu^+ \rightarrow e^+ + e^- + e^+, \qquad (4)$$

and

$$\mu^- + (Z, A) \rightarrow e^- + (Z, A). \qquad (5)$$

The experimental upper limits on these reactions are listed in Table IA.

Several processes, each allowed or preferred by only one conservation scheme, have been proposed. Muonium, anti-muonium conversions,

$$\mu^+ + e^- \rightarrow \mu^- + e^+, \qquad (6)$$

and colliding electrons producing muons,

$$e^- + e^- \rightarrow \mu^- + \mu^-, \qquad (7)$$

are permitted by the use of a multiplicative muon number. Attempts at observation of these processes present formidable experimental problems and to date only large upper limits on the ratio of the hypothetical coupling constants to the vector coupling constant, G_V, have been obtained (see Table IB).

Pontecorvo[3] has suggested that the reactions in Table IA may be favored if the lepton number (L) takes the value L=2 for the (μ^-, ν_μ) pair and L=1 for the (e^-, ν_e) pair, since these reactions would involve $\Delta L=1$ transitions, whereas the reactions listed in Table IB would have $\Delta L=2$.

He has also discussed[3] the reaction of muon capture with

TABLE I

SOME HYPOTHETICAL SEMI-LEPTONIC AND LEPTONIC REACTIONS

A. Reaction	Branching Ratio
$\mu^+ \rightarrow e^+ + \gamma$	$< 2 \times 10^{-8}$ [4]
$\mu^+ \rightarrow e^+ + e^+ + e^-$	$< 1.5 \times 10^{-7}$ [5]
$\mu^- + Z \rightarrow e^- + Z$	$< 2.2 \times 10^{-7}$ [6]

B. Reaction	Coupling Constant
$\mu^+ + e^- \rightarrow \mu^- + e^+$	$G/G_V < 5800$ [7]
$e^- + e^- \rightarrow \mu^- + \mu^-$	$G/G_V < 610$ [8]

positron emission,

$$\mu^- + (Z, A) \rightarrow e^+ + (Z-2, A). \qquad (8)$$

If observed, this reaction could select the conservation law with a single additive lepton number. It is an experimental search for this process which forms the subject of this thesis.

CHAPTER II

THEORY

In order for Reaction (8) to proceed, a charge exchange of two units ($\Delta Q = 2$) must occur. Thus, if the nucleus were composed exclusively of neutrons and protons, a process of second order would have to be considered. However, experiments have indicated that baryon resonances are also present in complex nuclei with probabilities of the order of 1% for the least massive resonances.[9] Theoretical investigations of the existence in nuclei of baryon resonances, such as the $\Delta(1236)$, have also indicated probability components of a few per cent.[10] The $\Delta(1236)$ is the pion-nucleon resonance with spin $J = 3/2$ and isospin $I = 3/2$. Since the $\Delta(1236)$ has four charge states (2, 1, 0, -1), it is possible to envision a first order, $\Delta Q = 2$, weak process for Reaction (8).[3] Figure 1 shows such a process, which has as its initial state two protons (p) and a negative muon. In the intermediate state is formed the $\Delta(1236)$ with charge q, which interacts with the negative muon, producing the $\Delta(1236)$ with charge q-2 and a positron. The final state consists of a positron and 2 neutrons (n).

Following the procedure of Primakoff[11] in his theory of muon capture, for which the nuclear charge change is $\Delta Q = 1$, Kisslinger[12] has calculated the branching ratio

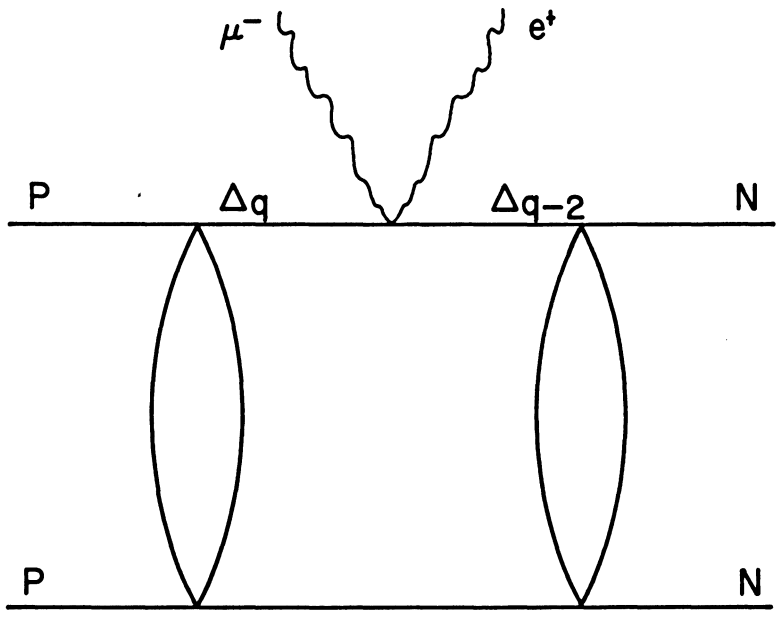

FIGURE 1

POSSIBLE FEYNMAN DIAGRAM FOR $\mu^- + Z \longrightarrow e^+ + Z - 2$

for Reaction (8) relative to ordinary muon capture in copper. Here, the effective Hamiltonian for Reaction (8) is assumed to have the same form as the $\Delta Q = 1$ process:

$$H_{eff}^{\Delta Q=2} = G_{\Delta} \left[(1 - \hat{\nu} \cdot \bar{\sigma}) / 2 \right] \tau^{2+} \sum_{i=1}^{A} I_i^{(2)-}, \qquad (9)$$

where G_{Δ} is the coupling constant for this $\Delta Q = 2$ interaction, τ^{2+} changes a μ^- state to an e^+ state, and $I_i^{(2)-}$ is a $\Delta Q = 2$, rank two, baryon-isospin step down operator. $\hat{\nu}$ is a unit vector in the direction of the e^+ momentum and $\bar{\sigma}$ is the Pauli spin operator. This Hamiltonian can be derived from a pion core model of the $\Delta(1236)$.[13]

Using a probability component $(a_{\Delta})^2 = 0.0075$[14] for the $\Delta(1236)$ in the copper nucleus and the closure approximation of Reference 11, the branching ratio of Reaction (8), relative to Reaction (2), is

$$R = \frac{G_{\Delta}^2 a_{\Delta}^4 P_{2p} P_{2p \to 2n}}{P_p P_{p \to n} \left[G_V^2 + 3G_A^2 + G_p^2 - 2G_p G_A \right]} \qquad (10a)$$

$$= (2.6 \times 10^{-6}) \left(G_{\Delta} / G_V \right)^2, \qquad (10b)$$

where $P_p = Z / A$, $P_{2p} = Z (Z - 1) / A (A - 1)$ are the probabilities for finding a proton and a proton pair, respectively, in the nucleus and $P_{p \to n} = 1 - 3(A - Z) / 2A$ and $P_{2p \to 2n} = 1 - 3(A - [Z - 1]) / 2A$ are the probabilities of transforming a proton into a neutron and two protons into two neutrons.[11] G_V, G_A, and G_p are, respectively, the vector, axial vector,

and pseudoscalar coupling constants. The calculation using the closure approximation includes all possible final states under the assumption that only the lowest energetically possible states give appreciable contributions.

For the case of a natural Cu target (constituents 69.09% Cu^{63}, 30.91% Cu^{65}),[15,16] this assumption implies a transition from the ground state of Cu to the ground state or low lying state of Co. In this experiment, Cu^{63} is the preferred component, since Co^{63} has a stable ground state which is ΔE_{gs} = 3.6 MeV[16] higher than the ground state of Cu^{63}. A coherent transition in Reaction (8), one from the ground state of Cu^{63} to the ground state of Co^{63}, would result in a positron of energy, $E_{e+} = m_{\mu}c^2 - \Delta E_{gs} \simeq 102$ MeV, where m_{μ} is the muon mass and c is the velocity of light. However, since Co^{65} does not exist as a stable nuclear configuration, we might expect the final state in Reaction (8) to be Co^{64} + n, if Cu^{65} were the initial state. Then, the coherent process would have $\Delta E_{gs} \geq 15$ MeV[16] and would result in a positron of energy, $E_{e+} = m_{\mu}c^2 - \Delta E_{gs} \lesssim 90$ MeV.

Although there has been no previous search for this type of interaction, <u>per se</u>, the null result of the experimental search[6] for Reaction (5) is relevent. In this experiment, positrons were indistinguishable from electrons. Correcting this result, because a natural Cu target was used and only events with momentum P > 90 MeV/c were accepted, the branching ratio for Reaction (8) from this experiment is

$$R < 3.2 \times 10^{-7} \text{ (90\% confidence level)}$$

and the ratio of the coupling constants from Equation (10) is

$$(G_\Delta / G_V) < 0.35^{+0.17}_{-0.09} .$$

The limits on this ratio reflect the uncertainty in the value of a_Δ in Equation (10)

CHAPTER III

EXPERIMENTAL DETAILS

I. EXPERIMENTAL APPARATUS

The experiment was performed in two runs during January and September 1971. The first run served mainly to test the data taking system and to further define the sources of background which might limit the sensitivity of the experiment. In particular, we learned that it was desirable to be able to identify the particle emitted after muon capture as a positron, since protons with a wide range of energies are commonly emitted following muon capture.[17] Particle identification would also limit backgrounds of a purely accidental nature. Since 85% of the total data was accumulated in the September run, it is the setup for this run which will be discussed, noting relevent changes from the January run.

Physical Setup

The experimental apparatus is shown in Figure 2. The 100 MeV/c beam from the muon channel of the National Aeronautics and Space Administration Space Radiation Effects Laboratory synchrocyclotron was degraded by CH_2 and stopped in two copper targets (target 1, 1.36 gm/cm^2 and target 2, 0.886 gm/cm^2). A single target was used in the first run. S1 - S8 are scintillation counters and SC1 - SC8 are spark

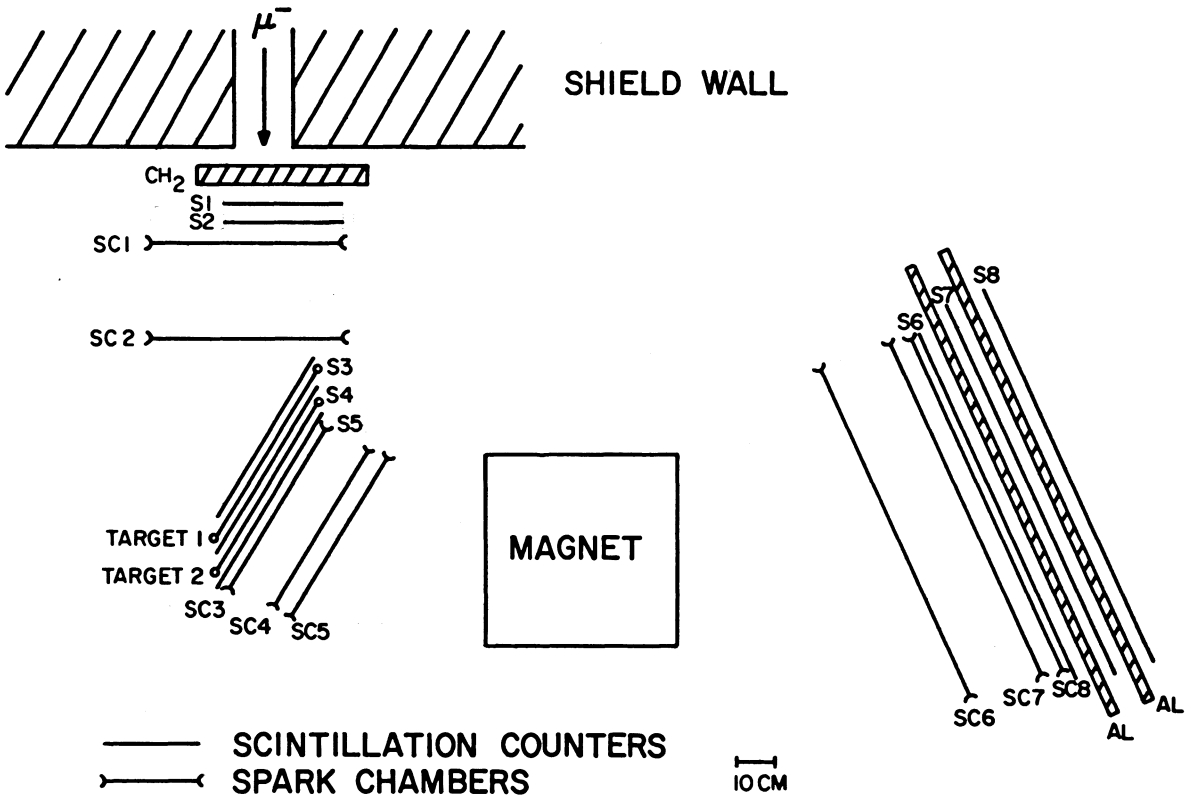

FIGURE 2

EXPERIMENTAL APPARATUS

chambers with magnetostrictive readouts. The dimensions of the scintillation counters were: S1 and S2: 30.5 cm x 30.5 cm x 0.635 cm; S3 and S4: 40.6 cm x 25.4 cm x 0.158 cm; S5: 40.6 cm x 25.4 cm x 0.316 cm; and S6, S7, and S8: 91.5 cm x 45.7 cm x 0.635 cm. The beam was defined by S1, S2, and S3 and the two targets were sandwiched between S3 and S4, and S4 and S5. The virtually pion-free beam consisted mainly of muons from the decay $\pi^- \rightarrow \mu^- + \bar{\nu}_\mu$, for which the muon is emitted in the backward direction in the pion center of mass system. The other constituents of this backward beam were electrons. The particle flux through S1 and S2 was $\approx 3.8 \times 10^5$/ sec.

Electronic Logic

The electronic signature for a stop in target 1 was a coincidence of S1, S2, and S3 in anti-coincidence with S4:

$$\text{Stop}_1 = S1 \cdot S2 \cdot S3 \cdot \overline{S4},$$

and in target 2:

$$\text{Stop}_2 = S1 \cdot S2 \cdot S3 \cdot S4 \cdot \overline{S5}.$$

The total average rate of stops was $\approx 1.36 \times 10^5$/sec.

After a stop, there was an electronic dead time of 10 nanoseconds (nsec), which resulted from the use of counters S4 and S5 as anti-coincidence components in the stop as well as coincidence components in the ensuing event. A stop sig-

nal initiated a 400 nsec gate, during which time a particle emerging from the target through the spectrometer would signify a potential event. The dead time and gate length represent a fraction, $f_1 = 0.862$, of the potential captures, since the mean disappearance time for muons in copper is 160 nsec.[18] The total fraction of muons which could be captured before the muons decayed is $f_2 = 0.92$,[18] if there were no dead time and an infinitely long gate.

Scintillation counters S6, S7, and S8 were located on the opposite side of the magnet from the targets. The full counter signatures for events emanating from the targets were

$$M_1 = A \cdot S6 \cdot S7 \cdot S8$$

for target 1 and

$$M_2 = B \cdot S6 \cdot S7 \cdot S8$$

for target 2, where $A = Stop_1 \cdot \overline{S1} \cdot \overline{S2} \cdot \overline{S3} \cdot S4\ S5$ and $B = Stop_2 \cdot \overline{S1} \cdot \overline{S2} \cdot \overline{S3} \cdot \overline{S4} \cdot S5$. A block diagram of the logic producing these signals is given in Figure 3A and the timing relationships for the components of M_1 are shown in Figure 3B. The average rates for M_1 and M_2 were 7.6×10^{-3}/sec and 7.2×10^{-3}/sec, respectively.

Aluminum absorbers (3.4 gm/cm^2) were placed between S6 and S7, and S7 and S8, to eliminate protons emitted following muon capture. However, a proton might stop in one of the

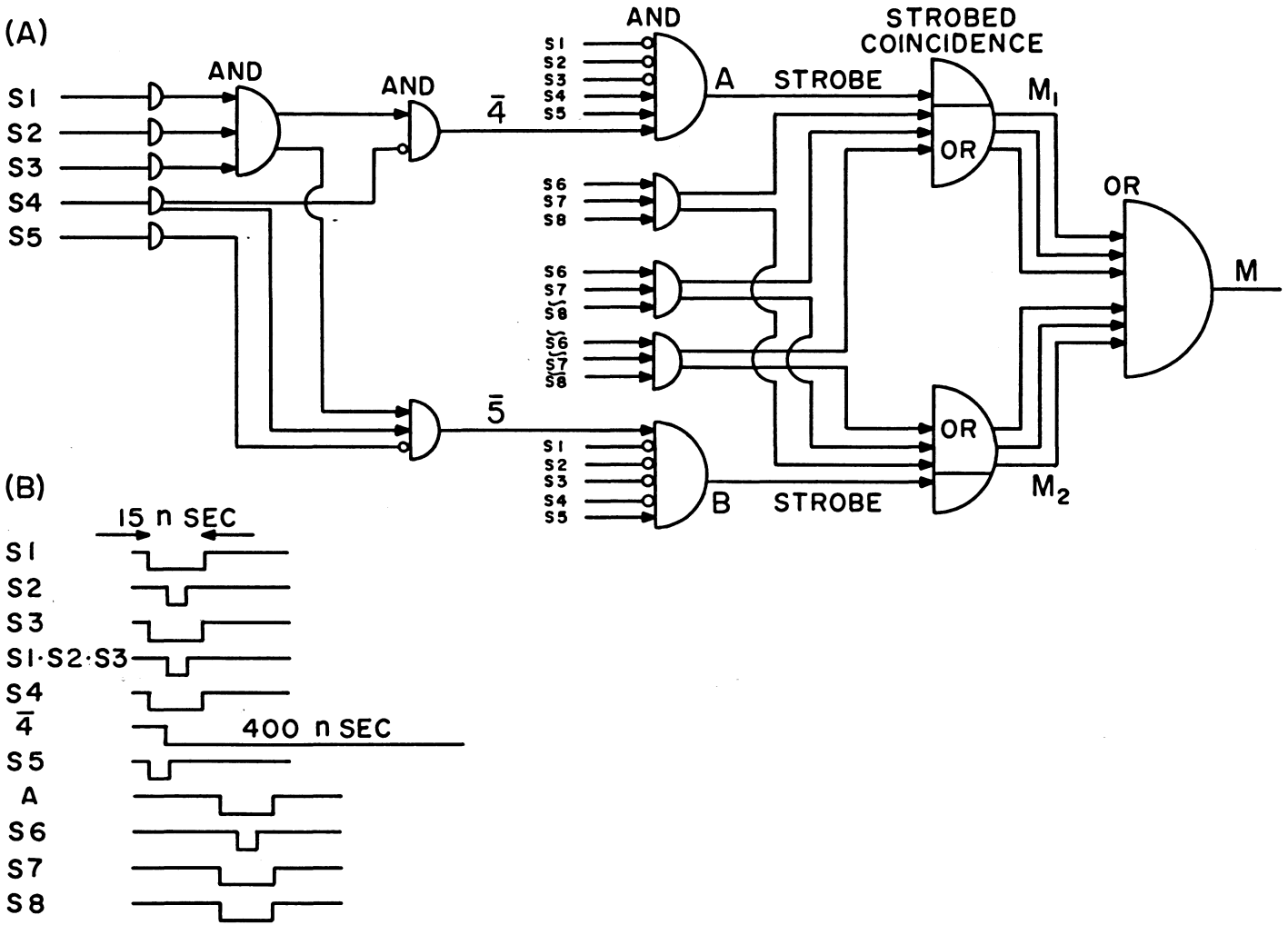

FIGURE 3

(A) BLOCK DIAGRAM OF LOGIC FOR M (B) TIMING RELATIONSHIPS FOR COMPONENTS OF M_1

absorbers in random coincidence with a count from S7 and/or S8. In order to monitor this type of accidental event, we counted signals such as

$$ACC1 = (A \text{ or } B)\cdot S6\cdot S7\cdot\widetilde{S8},$$

where the ($\sim$) over a coincidence component indicates a random time relationship. The average rate for ACC1 was $\approx 0.2 \times 10^{-2}$/sec.

We were also interested in the rates of events produced by unrelated particles on the two sides of the magnet, so we counted accidental coincidences

$$ACC2 = (A \text{ or } B)\cdot\widetilde{(S6\cdot S7\cdot S8)},$$

$$ACC3_1 = Stop_1\cdot\overline{S1}\cdot\overline{S2}\cdot\overline{S3}\cdot S4\cdot\widetilde{S5}\cdot S6\cdot S7\cdot S8,$$

and

$$ACC3_2 = Stop_2\cdot\overline{S1}\cdot\overline{S2}\cdot\overline{S3}\cdot\overline{S4}\cdot\widetilde{S5}\cdot S6\cdot S7\cdot S8.$$

The average rates for ACC2 and ACC3 were $\approx 0.1 \times 10^{-2}$/sec and $\approx 0.02 \times 10^{-2}$/sec, respectively.

Particle Identification

The most effective particle identification technique used was a measurement of the time of flight (TOF) between counters S5 and S6 for the particle emitted after a stop. This system was mainly intended to identify protons emitted following muon capture for which the velocities could range

up to V≃0.43c (maximum proton energy of ≃100MeV). The TOF system was calibrated in the direct beam (100 MeV/c, e^- and μ^-) and the variation of delay for light travel time was compensated for in both counters. Figure 4 shows the spectra obtained from electrons (V ≃ c) and muons (V ≃ 0.77c) at points in S5 and S6 closest to the photomultiplier tubes, when the separation between S5 and S6 was 2.34 meters (m). The electron peak and muon peak are separated by ≃4 nsec. For the most energetic protons from muon capture traversing the spectrometer (≃2.5m path length), the electron peak to proton peak separation would be ≃11 nsec. Since the heavy charged particle spectrum from muon capture is essentially exponentially decreasing[17] from a few MeV, we were confident that we could eliminate protons as a direct source of background.

We also measured the relative pulse height or energy loss in counter S6 (PH6) of the particles emitted after a stop. Figure 5 shows the spectra from traversal of the 100 MeV/c beam. The clear separation of the electron and muon peaks gave us a further indication of the ability to identify protons, since protons of momenta 100 MeV/c should give energy losses of the order of 10 times that of muons. However, this technique was not very useful in eliminating accidental type backgrounds, because of the large number of electrons which contributed to these backgrounds (see Section III of this chapter).

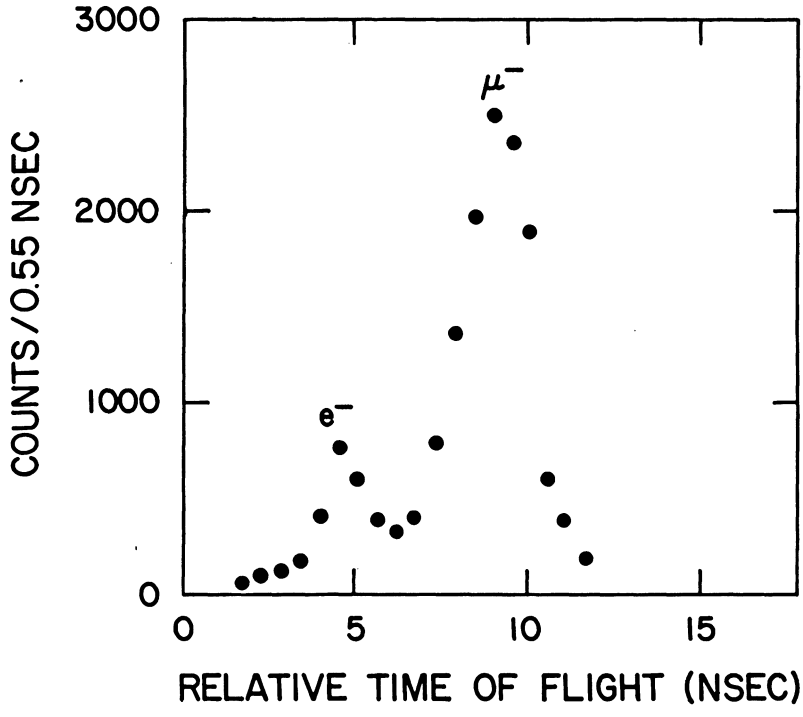

FIGURE 4

RELATIVE TIME OF FLIGHT (TOF) BETWEEN S5 AND S6 FOR ELECTRONS AND MUONS OF MOMENTUM 100 MeV/c FOR A COUNTER SEPA- OF 2.34 METERS

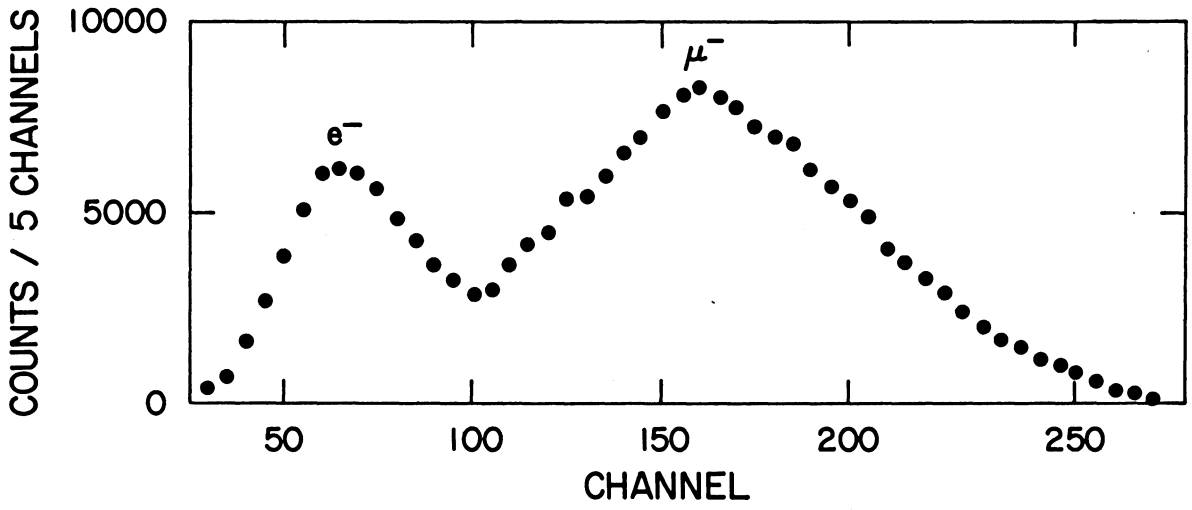

FIGURE 5

PULSE HEIGHT DISTRIBUTION IN S6 FROM TRAVERSAL OF THE 100 MeV/c BEAM

Event Time

In the January run, there was a 25 nsec delay after the muon stop before a 200 nsec gate was opened (allowing for a fraction, 0.610, of the captures to be detected). The delay was used to eliminate prompt, beam-related events. For the main data taking period (September), we replaced this with a direct measurement of the event time (EVT), the time between a stop and an event (in S5). This was useful in the evaluation of π^+ decay calibration data to be discussed below.

Spark Chamber System

The master signal, M, consisted of one of the "real" triggers, M_1 or M_2, defined above, or one of the "accidental" triggers, ACC1 or ACC2, from either target. The average rate for $M = M_1 + M_2$ was 1.48×10^{-2}/sec. Signal M served as the trigger for the spark chamber system.

The spark chamber system was made up of eight (six in the January run) magnetostrictive readout wire spark chambers filled with a flowing gas mixture (commercially available) of 90% Ne, 10% He. Each chamber had two perpendicular planes of 0.127 mm diameter copper wire, with an equal wire spacing of approximately two wires per mm, supported by a 1.0 cm thick Benelex or fiber glass window frame, and covered by 0.127 mm mylar windows. The dimensions of the active areas of the chambers SC1, SC2, SC3, SC4, and SC5 were 40.6 cm x 25.4 cm and for SC6, SC7, and SC8, 91.5 cm x 43.2 cm.

In each chamber, one plane of wires was kept at ground potential and the other plane was pulsed[19] by approximately 8 kiloVolts whenever the scintillation counter signal, M, fired. This indicated that a charged particle may have passed through the chambers. If a charged particle had left an ionized path in the gas of a chamber, a spark could have occurred across the path and current would have flowed in the wire (or wires) nearest the path in each plane.

Perpendicular to each plane of wires, at the extremity of the plane, was an insulated Ni-Co wire with magnetostrictive properties. The current-carrying spark chamber wire caused a magnetostrictive pulse in the Ni-Co wire, which propagated along the Ni-Co wire at a fixed velocity, thus localizing the spark position. The magnetostrictive pulse was picked up at the end of the Ni-Co wire by a receiving coil, which fed an amplifier attached to the chamber frame. The amplifier output was sent to a variable threshold discriminator-shaper.[20]

Each Ni-Co wire, corresponding to one plane of one spark chamber, was tied to a set of scalers that were run with 20 megaHertz clock pulses. The scalers were enabled by the trigger signal, M, and disabled by the signal(s) from the magnetostrictive wire. In this way, the propagation time of the magnetostrictive pulse was digitized.

A 250 Volt clearing field was applied between the planes of each chamber. The clearing field limits the chamber's

memory time by removing old particle tracks. For 250 Volts, we found that the sparking efficiency of a typical chamber was nearly constant at e ≃ 95% for tracks that were formed up to ≃0.4 microseconds (μsec) before the chamber was fired. The efficiency dropped to e ≃ 4% at ≃0.9 μsec.

The scalers for each chamber plane (four spark maximum) were scanned and read out sequentially to a data acquisition computer interface connected to an on-line IBM-360/44 computer. The computer transferred the raw data to magnetic tape and calculated the spark positions for each chamber. The TOF, PH6, and EVT data for each event were also fed through the interface to the on-line computer. The computer enabled us to monitor the performance of the spark chamber system and the EVT, PH6, and TOF spectra and to perform simple trajectory calculations for potential events.

Spark chambers SC1 and SC2 served mainly to define the beam spread on the targets and chambers SC3, SC4, SC5, SC6, SC7, and SC8 defined the trajectory of a particle passing through the magnet. The space between SC5 and SC6 was filled with a He-filled bag (windows, 0.051 mm thick mylar) to reduce the effects of multiple Coulomb scattering in air.

The spark chambers were attached to aluminum mounting frames that were pinned to leveled aluminum table tops placed on either side of the magnet. The relative position of the mounting frames to each other were measured to within 0.5 mm and the relative positions of the chambers and frames to

within 0.5 mm. The intrinsic resolution of the chambers was 0.5 mm. However, the errors introduced into the trajectory calculations from these uncertainties were small compared with those due to multiple Coulomb scattering in the chambers. Considering scattering from the wires of SC5 only (effective 0.06 gm/cm^2), we expected a rms projected scattering angle for a 100 MeV/c electron of $\theta_p = 2.1 \times 10^{-2}$ radians.[22] Projecting this to SC6 results in a displacement of ≈1 cm.

The analyzing magnet (pole pieces 50.8 cm x 50.8 cm and gap 35.6 cm) was operated at 4.0 kiloGauss (kG) in the first run. In the second run, this was reduced to 2.0 kG, so that the solid angle subtended by the spectrometer would remain large for particles of lower momenta. Relative values of the symmetric magnetic field were measured at 1680 points in one octant to within 0.5% accuracy using a three dimensional Hall probe.

Solid Angle

From a knowledge of the beam spread on the target, the average fractional solid angle was calculated by the Monte Carlo method using a square magnetic field approximation. Target positions, weighted according to the experimentally determined beam distribution, were chosen at random, followed by random selection of the outgoing direction for a given momentum. The trajectory was then traced to see if the particle would successfully pass through the spectrometer to

the last counter. The average fractional solid angles subtended by the spectrometer for momenta 30-110 MeV/c calculated in this manner for the muon beam distribution are given in Figure 6. At the momentum 100 MeV/c, the fractional solid angle was

$$\Delta\omega/4\pi = (6.1 \pm 0.6) \times 10^{-3}.$$

II. CALIBRATION AND DATA TREATMENT

Event Selection Criteria

Since we were searching for a rare, perhaps nonexistent, process, it was important to establish criteria for acceptance of an event. The first condition, of course, was placed on the momentum. The momentum was determined by reconstructing the particle's trajectory through the magnetic field and calculating an effective radius of curvature. Two points on each side of the magnet were obtained from chambers SC3 and SC4 or SC5, and SC6 and SC7 or SC8. A "best" trajectory was then calculated by an iterative method,[23] which simultaneously performed a least squares fit to the spark chamber points in the horizontal and vertical directions. The question of "goodness of fit" criteria can best be discussed in terms of the horizontal and vertical residuals (Rx and Ry), which are the differences in the horizontal and vertical planes, respectively, between the fitted and actual positions. These deviations from a perfectly fit trajectory were due to

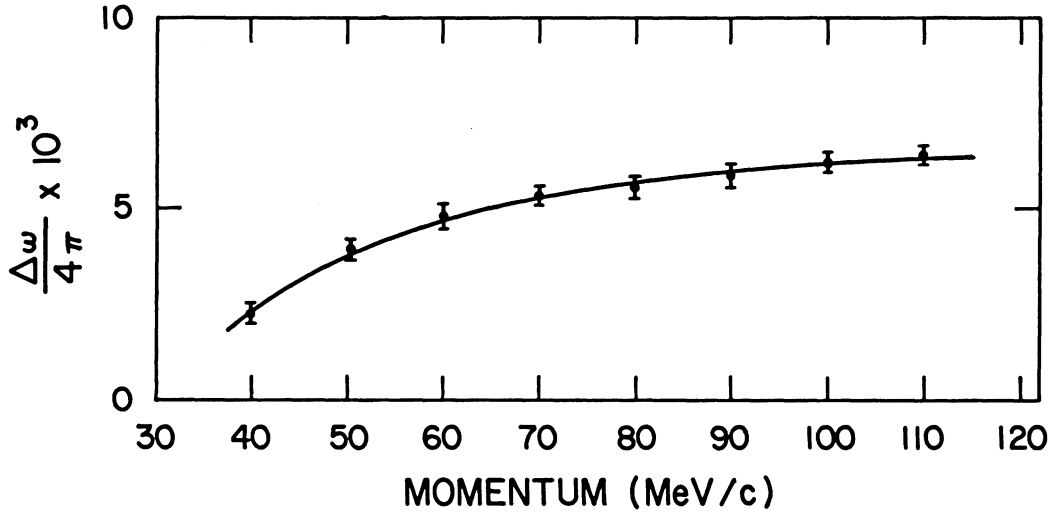

FIGURE 6

AVERAGE FRACTIONAL SOLID ANGLE SUBTENDED BY THE SPECTROMETER FOR THE MUON BEAM DISTRIBUTION

position uncertainties, intrinsic resolution of the chambers, multiple Coulomb scattering, and imperfect knowledge of the magnetic field.

Standards for the residuals were obtained by using positrons from decays of positively charged muons and pions. In order to have a positive beam in the muon channel, we reversed the proton current in the cyclotron (by reversing the polarity of the main field), so that the production target was struck from the opposite direction. The pions which stopped in the copper targets decayed mainly to muons ($\pi^+ \rightarrow \mu^+ + \nu_\mu$), which subsequently decayed producing positrons (Reaction [1]) with momenta ranging up to a maximum of 53 MeV/c. The pions also decayed to positrons ($\pi^+ \rightarrow e^+ + \nu_e$) with a branching ratio of $\simeq 1.25 \times 10^{-4}$.[24] A positron from pion decay has a unique momentum, 70 MeV/c.

Plots of the residuals for events with calculated momenta 35 ± 5 MeV/c, 45 ± 5 MeV/c, 55 ± 5 MeV/c, 65 ± 5 MeV/c, and 125 ± 15 MeV/c are shown in Figure 7 for the horizontal distributions and Figure 8 for the vertical distributions. The distribution labeled 125 ± 15 MeV/c in each figure was due to pions elastically scattered from one of the targets. Since the rms projected angle due to multiple Coulomb scattering is inversely proportional to the product of momentum and velocity,[22] $\theta \propto (P \cdot V)^{-1}$, pions of momentum P = 125 MeV/c and velocity V = 0.68c and positrons of momentum P = 85 MeV/c and velocity V ≃ c have similar multiple

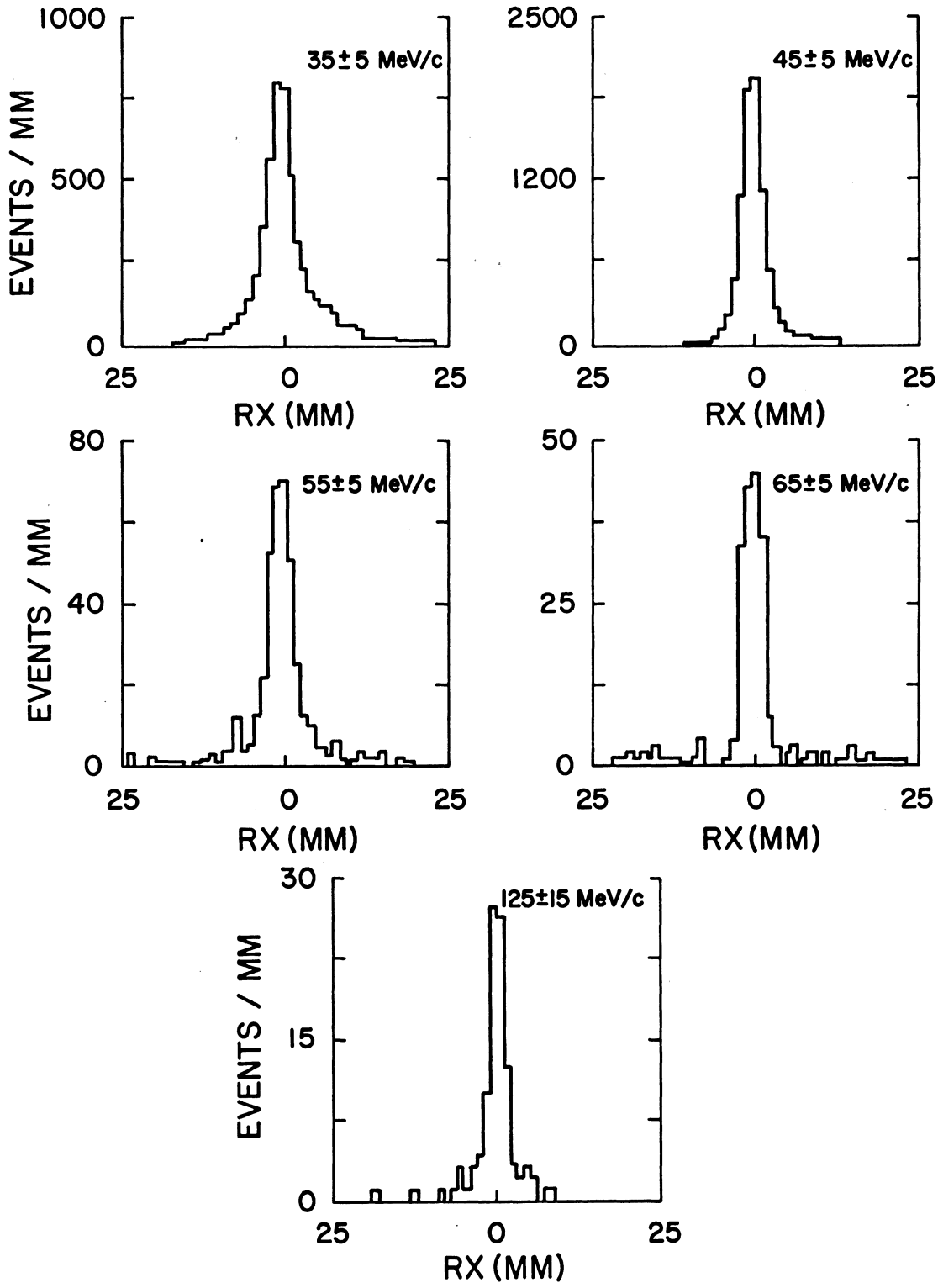

FIGURE 7

HORIZONTAL RESIDUAL DISTRIBUTIONS

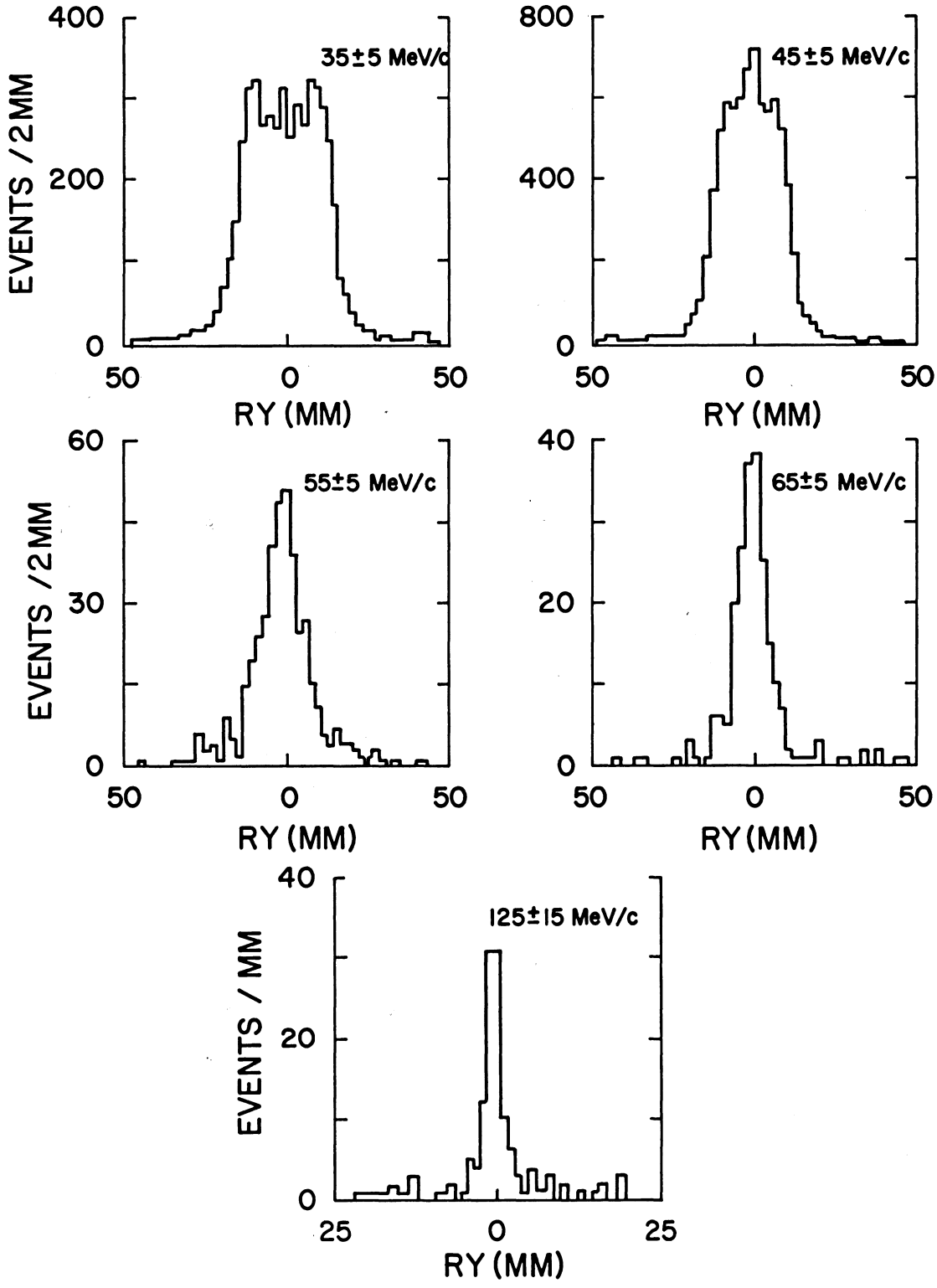

FIGURE 8

VERTICAL RESIDUAL DISTRIBUTIONS

scattering characteristics.

These histograms all have long, flat tails, due to low energy positrons which underwent severe multiple scattering to produce trajectories that were fit poorly as higher (or lower) momenta. For instance, from a near-perfect trajectory, a 1 cm displacement at one of the four chambers would produce horizontal residuals of about 0.3 cm at all of the chambers and change the momentum of a 75 MeV/c particle by 15%.

The existence of these tails presented a problem for setting "acceptability"limits on the residuals, especially for the momentum regions greater than 50 MeV/c, where the statistics were low. To overcome this, self-consistency requirements were placed on the data sets, noting that the average displacements due to multiple Coulomb scattering should be inversely proportional to momentum for electrons. For the horizontal residual distribution at 35 ± 5 MeV/c, full width at half maximum (FWHM) ≈4.6 mm, all data within the limits ±20 mm were used. Then the residual values, within which 98% of this data were included, were determined. For the next region, 45 ± 5 MeV/c, any residuals outside the 98% limits of the 35 MeV/c region were excluded as spurious. For example, 98% of the data within ±20 mm in the 35 ± 5 MeV/c horizontal residual distribution was contained within ±15.5 mm. Then, for the 45 ± 5 MeV/c horizontal residual distribution, no residual was included that had a value $|Rx| > 15.5$ mm.

98% of these residuals had values $|Rx| < 0.95$ cm. The limits obtained in this way are plotted in Figure 9. As expected, except for the first value, at 35 ± 5 MeV/c, which is somewhat arbitrary, the widths are inversely proportional to momentum. The horizontal widths are generally less than the vertical, since the horizontal plane trajectory is overdetermined by one variable and the vertical plane trajectory by two.

We believe that these limits are sufficiently large to include virtually all the real data in these momentum regions. For instance, for the horizontal residual distribution at 125 ± 15 MeV/c (representing positrons at 85 ± 15 MeV/c), the FWHM ≃ 2.5 mm. The limit, $|Rx| < 5.5$ mm, represents ≃ 4.5 FWHM.

Calibration of the Momentum Scale

The absolute momentum scale and resolution were determined using the 70 MeV/c positrons from $\pi^+ \rightarrow e^+ + \nu_e$ decays. Assuming that the pion stops were equally distributed throughout the target thicknesses, we expected a positron energy loss[25] from bremsstrahlung and collision processes for the stops in the first target to be $\Delta E_1 = 12.1 \pm 4.4$ MeV. For the second target we expected $\Delta E_2 = 4.9 \pm 3.0$ MeV. The observed spectra for both targets, shown in Figure 10, were consistent with these expectations. They give $\Delta E_1 = 9 \pm 6$ MeV and $\Delta E_2 = 6 \pm 3$ MeV. An event was considered to be due to

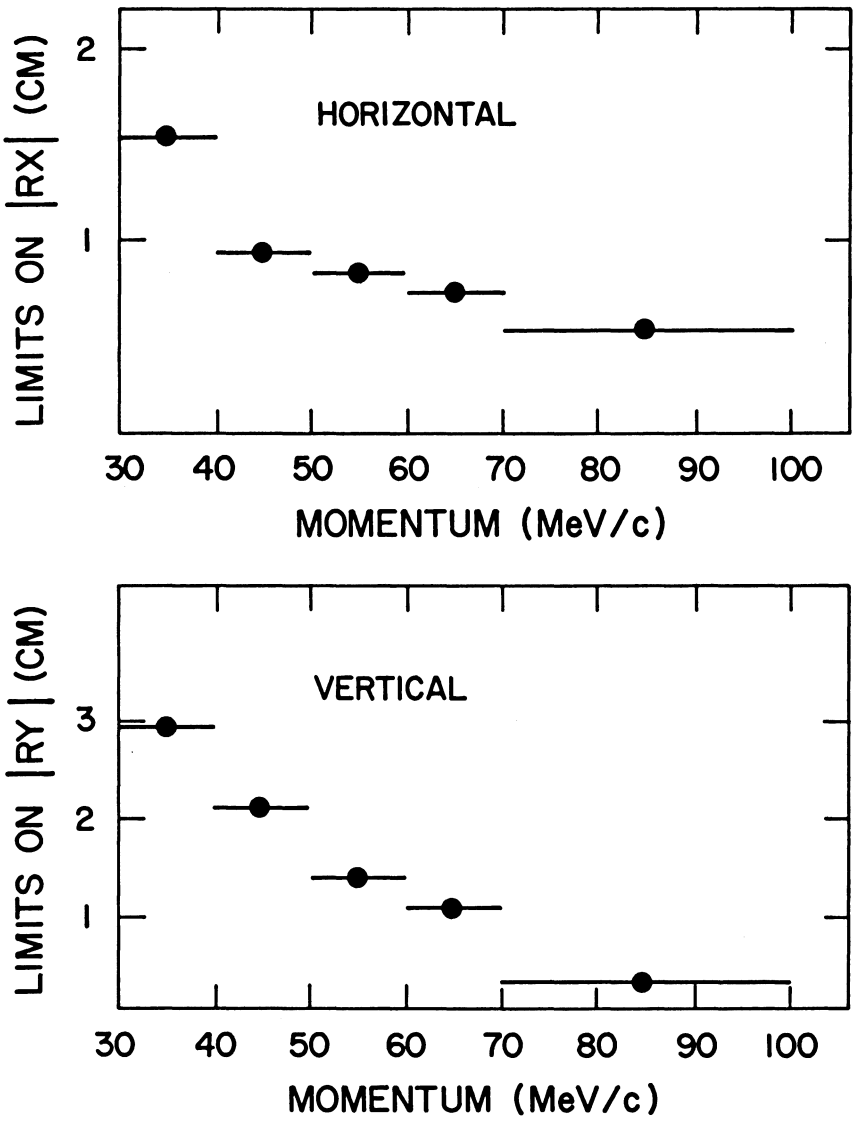

FIGURE 9

LIMITS ON RESIDUALS FOR ACCEPTABLE EVENTS

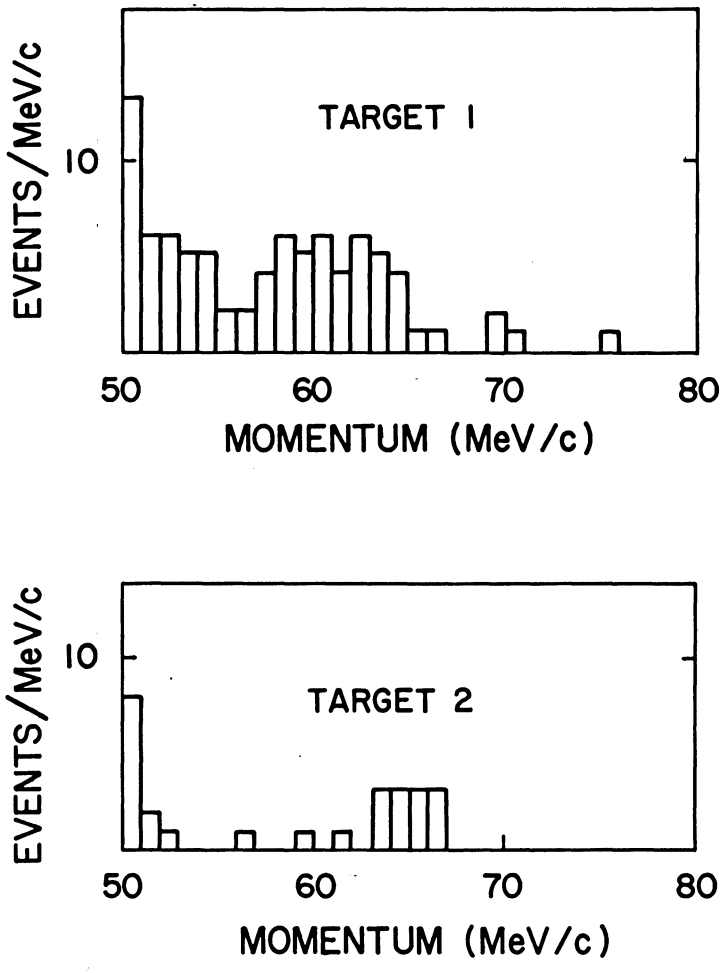

FIGURE 10

MOMENTUM DISTRIBUTION OF POSITRONS FROM PION DECAY

the decay $\pi^+ \rightarrow e^+ + \nu_e$ if the momentum of the detected positron was in the region $54 < P_{e^+} < 66$ MeV/c for target 1 and $61 < P_{e^+} < 67$ MeV/c for target 2. In Figure 10, the regions below ≈54 MeV/c for target 1 and ≈61 MeV/c for target 2 contain positron events from decays of pions which stopped in counters S3 and S4, respectively, and from positrons with near maximum energy from muon decay (Reaction [1]).

Using the $\pi^+ \rightarrow e^+ + \nu_e$ data, we set our momentum resolution at $\Delta P/P \simeq 10\%$ for target 1 and $\Delta P/P \simeq 5\%$ for target 2. We then found that a positron of momentum 102 MeV/c should appear in the ranges 86 ± 8 MeV/c and 94 ± 4 MeV/c for targets 1 and 2, respectively.

Detection Efficiency

The minimum conditions for reconstructing a trajectory were single sparks in at least four of the required chambers (SC3 and SC4 or SC5, and SC6 and SC7 or SC8). The preferred combination was SC3, SC5, SC6, SC8, because this offered the widest separation between trajectory points. After subtraction of the accidental trigger background, we found the average efficiency (including the scintillation counters and at least four of the required chambers) for detection of a positron after a stop was

$$E_{ff} = 75.5 \pm 7.0\%.$$

Runs with a positive beam in the muon channel were done four

times during the September experiment, before and after approximately each third of the μ^- data was taken. The efficiency was constant in these runs to within 10%.

Overall Check of the System

As a calibration check on the detection system, we measured the $(\pi^+ \rightarrow e^+ + \nu_e) / (\pi^+ \rightarrow \mu^+ + \nu_\mu)$ branching ratio in the last positive beam run ($\simeq$ 4 hours). In comparison with the value obtained in the most recent full-scale measurement of this branching ratio,[24] $R_{\pi e} = (1.247 \pm 0.028) \times 10^{-4}$, we found

$$R_{\pi e} = \frac{N_{\pi e}}{N_\pi \, (\Delta\omega/4\pi)_{\pi e} \exp(-\lambda_\pi t_0)(1 - \exp[-\lambda_\pi t_1]) \, E_{ff}}$$

$$= (0.8 \pm 0.3) \times 10^{-4},$$

where:

$N_{\pi e} = 16$ is the number of events attributed to $\pi^+ \rightarrow e^+ + \nu_e$ decay in the targets. These events were detected in the time period $t_1 = 30$ nsec, beginning after time $t_0 = 10$ nsec. The TOF, PH6, and EVT spectra of these events were consistent with those expected for positrons from pion decay;

$(\Delta\omega/4\pi)_{\pi e} = (5.5 \pm 0.6) \times 10^{-3}$ is the average fractional solid angle for positrons of original energy 70 MeV, calculated using the pion beam distribution on the targets;

. λ_π is the pion decay constant;

$E_{ff} = 0.755 \pm 0.070$ is the detection efficiency;

$N_\pi = (1.1 \pm 0.2) \times 10^8$ is the number of pions that stopped in the targets. N_π was determined from the EVT spectrum of particles detected after pion stops. This spectrum, with the random background subtracted, is shown in Figure 11. In the figure, the peak at time t = 0 is the result of the inefficiency of the veto counters (S4 and S5) in the stop signals. The counters missed particles elastically scattered from the targets. Following the electronic dead time, which ends at $t_0 \simeq 10$ nsec, are events due to decays of muons that resulted from the decays of the stopping pions. A least squares fit of this data was performed for N_T, the total number of pions stopping in the targets and counters, using the following formula for the number of electrons detected during the time period, τ, beginning a time t_0 after the arrival of the pions:

$$N_e = N_T \{R_{\pi e} (\Delta\omega/4\pi)_{\pi e} \exp(-\lambda_\pi t_0)(1 - \exp[-\lambda_\pi \tau])$$

$$+ (\Delta\omega/4\pi)_{\mu e} \frac{\lambda_\pi \lambda_\mu}{\lambda_\pi - \lambda_\mu} [(1 + f) \frac{\exp(-\lambda_\mu t_0)}{\lambda_\mu} (1 - \exp[-\lambda_\mu \tau])$$

$$- \frac{\exp(-\lambda_\pi t_0)}{\lambda_\pi} (1 - \exp[-\lambda_\pi \tau])]\},$$

where $(\Delta\omega/4\pi)_{\mu e} = (1.8 \pm 0.2) \times 10^{-3}$ is the average fractional solid angle weighted according to the momentum distribution for positrons from the decay $\mu^+ \rightarrow e^+ + \nu_e + \bar{\nu}_\mu$, λ_μ is the

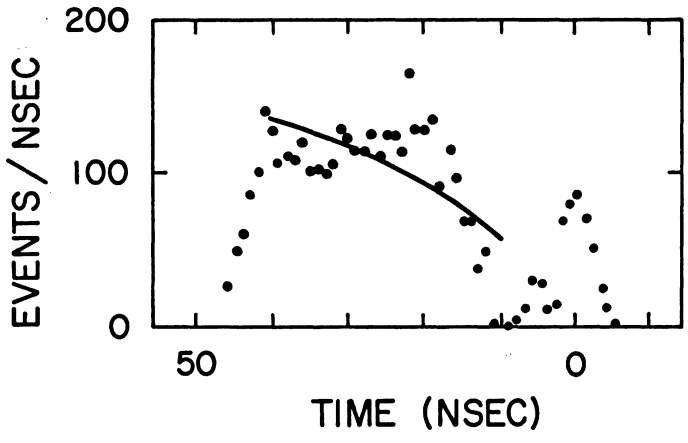

FIGURE 11

EVENT TIME SPECTRUM FOR PARTICLES DETECTED AFTER PION STOPS (GATE LENGTH WAS 50 NSEC)

muon decay rate, and f allows for an estimated 5% muon contamination in the pion beam. The number of pions that stopped in the targets was experimentally determined to be 57% of N_T.

III. EXPECTED BACKGROUND

With a high muon stop rate and a relatively long gate initiated by each stop, we were led to consider the problem of accidental processes and real processes which might be confused with an event from the process $\mu^- + Cu \rightarrow e^+ + Co$.

Particles scattered from the negative beam after a muon stop were eliminated by the wrong sign of their momentum and by using counters S1, S2, S3, and S4 in anti-coincidence. Charged particles emitted from a target following a muon stop were a more subtle background. 8% of the captured muons eventually decay yielding electrons and about 15% of the captures yield heavy charged particles[17] (protons, deuterons, tritons). The electrons had the wrong charge and low momentum, but could create a track in the spark chambers before the magnet. Uncorrelated tracks on both sides of the magnet could simulate a connected trajectory. From a background run where the trigger was S6·S7·S8, we found that the rate of production of random tracks behind the magnet was ≈ 2/sec. It was then possible to calculate the number of expected, randomly produced events of any momentum which would fall within the residual limits of a 70 MeV/c particle. This was < 0.01 for the entire experiment.

The protons emitted following muon capture presented a different type of problem, since they had the same charge as positrons and had a wide momentum range spanning the region of interest.[17] The aluminum absorbers between S6 and S7, and S7 and S8 eliminated these from making real triggers. The time of flight and energy loss information were additional factors in the expected background number of < 0.01 events.

The most significant form of background in the experiment was from the process of radiative muon capture,

$$\mu^- + Cu \rightarrow \nu_\mu + \gamma + Ni. \qquad (11)$$

The photon, for which the energy can range up to a maximum of between 90 and 100 MeV, can convert in the target, producing an (e^+, e^-) pair. The e^-, which got only a small fraction of the photon's energy, would be stopped in the target, with the remainder of the photon's energy going to the e^+. If the e^- received more than $\simeq$ 3.5 MeV in target 1 or $\simeq$ 1.5 MeV in target 2, it would nullify the event by the anti-coincidence conditions on S3, or S4, or by way of producing a second spark in SC3 (and possibly SC4 and SC5). The total branching ratio for Reaction (11), relative to ordinary muon capture, is $R = (4.9 \pm 1.1) \times 10^{-4}$.[26] For the region with photon energy $E_\gamma > 50$ MeV, the partial branching ratio reported is $R_p = (1.20 \pm 0.18) \times 10^{-4}$.[26] From a calculation to be described in relation to the observed data (see Chapter IV),

we expected to observe approximately 10 positrons in the range 40 to 80 MeV/c.

Other processes were also considered as possible sources of background. Assuming that there was < 1% π^- contamination in the muon beam, we calculated that the process of π^- absorption on a nucleus producing a high energy photon would result in < 0.01 events that might be attributed to Reaction (8). We also expected < 0.01 background events from radiative muon decay,

$$\mu^- \rightarrow e^- + \bar{\nu}_e + \nu_\mu + \gamma. \qquad (12)$$

Although Reaction (12) should not have been the cause of any events that could be confused with Reaction (8), we calculated that of the order of 2.5×10^3 spark chamber triggers (M) would result from events for which the electron from Reaction (12) fired S5 (and possibly S4) and the photon converted to an (e^+, e^-) pair before (or in) S6 to complete the trigger logic. We also anticipated triggers due to neutrons emitted following muon capture. Neutrons can fire the scintillation counters by knocking protons out of nuclei, but can create no spark chamber tracks. Other sources of triggers were events of a purely accidental nature (see Chapter III Section I) and those due to electrons from muon decay, which scattered from the magnet walls to complete the event signature. These electrons were expected to produce spark chamber tracks that could not be reconstructed

as acceptable events. In total, from these various sources of background, we calculated that < 0.01 events should be observed during the experiment which might appear to be due to Reaction (8).

CHAPTER IV

RESULTS

During the September run, we recorded a total number of 9.202×10^{10} stops. 52% of these were actual stops in the copper targets and the remainder either stopped in counters S3 and S4 or scattered out from the targets. The efficiency for rejecting beam particles that passed through the targets, but did not stop in them, was 97.5%. These factors resulted in a total muon stop count in the Cu targets of

$$N_{\mu} = 4.665 \times 10^{10}.$$

There were 9309 spark chamber triggers (M) and 938 of these fired at least four of the required chambers (see Chapter III Section I). The fraction of triggers which were not accompanied by successful spark chamber tracks were due to the random and neutral types of background discussed earlier (see Chapter III Section III). Almost all of those events which fired the required chambers were evidently due to scattered electrons from muon decay and the combination of electrons and converting photons from Reaction (12). The TOF and PH6 spectra for these were generally consistent with that of the positrons from μ^+ decay. However, after placing the horizontal and vertical residual requirements imposed by the pion and muon decay data (see Chapter III Section II),

we were left with only the 11 events listed in Table II. In the first column of Table II are the observed momenta. The targets from which the events originated are given in the second column. The third column lists the momenta of the events with the average expected energy losses from collisions and bremsstrahlung restored.

All of the events listed in Table II had TOF and PH6 values consistent with those obtained using electrons in the 100 MeV/c beam and the EVT values were all > 60 nsec. An event was not included in the table if any of the six spark chambers (SC3-SC6) had more than one spark.

The event at 83.9 MeV/c from target 2 is of particular interest, because of its high momentum. This event fired all six spark chambers and the momentum calculated using six chambers is within 0.6 MeV/c of that calculated using the minimum four required. The horizontal residuals fall well within the acceptability limits. However, one of the vertical residuals has a value approximately equal to the upper limit for the 85 ± 15 MeV/c region. Because of the low statistics in the calibration data for this region, we felt that this event should be included.

To compare the observed spectrum with the anticipated background, we calculated the expected number and distribution of positrons from conversion of radiative muon capture photons for the case in which the electron received insufficient energy to reach SC3. The following procedure was used:

TABLE II

EVENTS FOR WHICH THE RESIDUALS
MEET THE ACCEPTABILITY REQUIREMENTS

Raw Data Momentum (MeV/c)	Target	Data With Energy Loss Restored Momentum (MeV/c)
38.5	2	41.9 ± 1.9
43.6	2	47.3 ± 2.1
43.0	1	52.6 ± 4.1
44.8	1	54.9 ± 4.2
83.9	2	89.9 ± 3.5
42.4	1	52.0 ± 4.0
53.0	1	64.4 ± 4.8
42.0	1	51.5 ± 4.0
40.6	1	50.0 ± 4.0
46.1	1	56.2 ± 4.3
38.1	1	47.0 ± 3.9

(1) The number and distribution of photons expected from radiative muon capture were calculated in the range $50 < E_\gamma < 91$ MeV in steps of 2 MeV. This was done by normalizing a linear approximation of the theoretical spectrum of Rood and Tolhoek[27] for $50 < E_\gamma < 91$ MeV to the experimental result of Chu *et al.*,[26] $R_p = (1.20 \pm 0.18) \times 10^{-4}$.

(2) For each photon energy region (2 MeV), the probability for producing an (e^+, e^-) pair was calculated for cases with electron energies $E_{e^-} \leq 3.5$ MeV (target 1) and $E_{e^-} \leq 1.5$ MeV (target 2), using the Bethe-Heitler equations.[22]

(3) The number of expected photons for each 2 MeV region was multiplied by the calculated conversion probability. This product was then multiplied by the proper solid angle factor for the corresponding positron momentum, after average energy losses from collisions and radiation were subtracted.

In the regions R1 (36.7 ± 6.5 MeV to 72.3 ± 9.5 MeV) for target 1 and R2 (45.9 ± 3.5 MeV to 85.1 ± 5.5 MeV) for target 2, the number of positrons expected from conversions of photons with energy $50 < E_\gamma < 91$ MeV was 8.7 ± 3.0 and 1.0 ± 1.0. We observed 8 events in R1 and 2 in R2.

The observed positron distributions from the two targets are histogrammed in Figure 12. The solid lines are the distributions calculated from radiative muon capture, as described above. Only the event from target 2, at 83.9 MeV/c, seems to be inconsistent with radiative muon capture. The calculated number of expected events with momentum

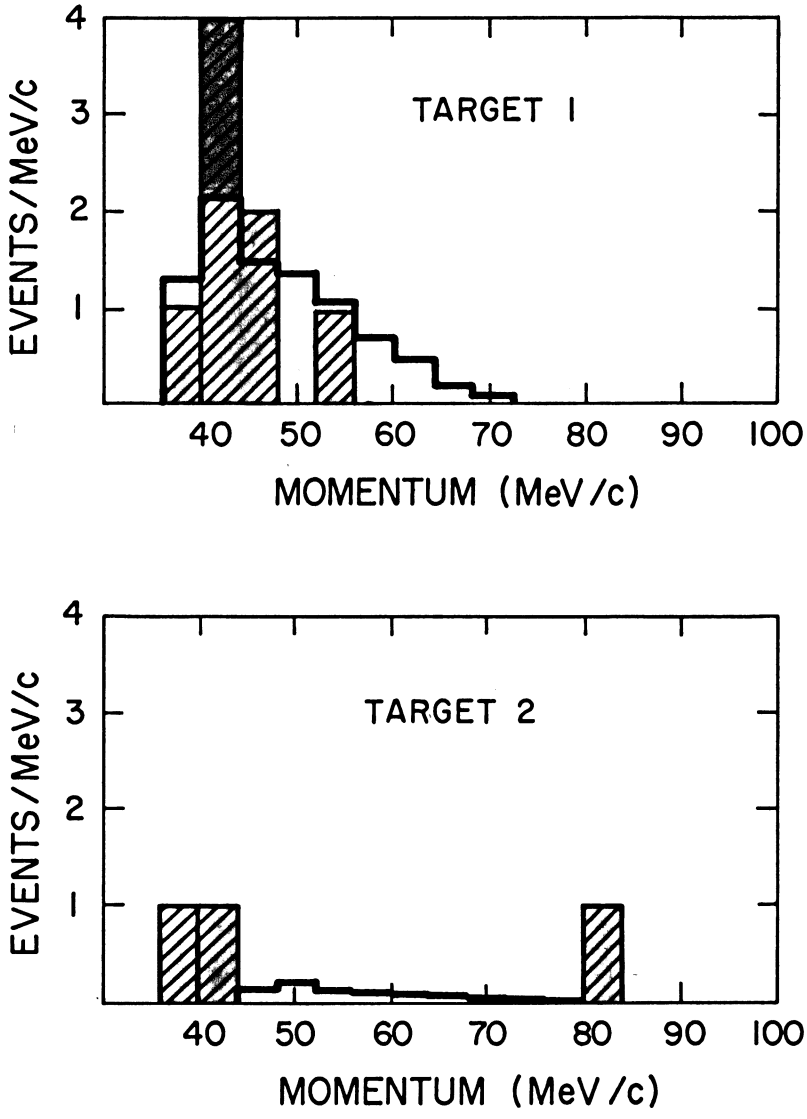

FIGURE 12

THE OBSERVED POSITRON SPECTRA (HATCHED) AND THE CALCULATED SPECTRA FOR POSITRONS FROM CONVERSION OF RADIATIVE MUON CAPTURE PHOTONS WITH ENERGY $50 < E_\gamma < 91$ MeV (SOLID LINE)

$P > 79.5$ MeV/c from target 2 is 0.013. If we assume that the maximum photon energy is $E_{max} = 100$ MeV, then this number would be 0.037 events. It should be noted that in the radiative capture experiment of Chu *et al.*[26] an enhancement of the photon spectrum at the upper end was observed, although the authors speculated that its origin may have been a background fluctuation. A recent radiative muon capture experiment[28] in Ca^{40} indicates no such enhancement.

The event at momentum 83.9 MeV/c is consistent with the process $\mu^- + Cu^{65} \rightarrow e^+ + Co^{64} + n$, for the case in which the e^+ has acquired near maximum energy, $\simeq$ 90 MeV. A positron of momentum 90 MeV/c from target 2 would be expected to fall in the region 84 $\pm$ 4 MeV/c. This event is probably not due to a ground state transition in the reaction $\mu^- + Cu^{63} \rightarrow e^+ + Co^{63}$. However, it does merit further consideration for the Cu^{63} case, because of the possibility of a nuclear excitation of 10 or 20 MeV to a giant resonance state. The importance of effects of giant dipole resonances in muon capture has been investigated theoretically by Foldy and Waleka.[29] Capture rates for A = 4N nuclei, calculated using the giant resonance model, agree well with experiments.[30] The giant resonance model has also been applied to radiative muon capture.[31]

Since we have observed only one event consistent with Reaction (8) and since there exists some uncertainty in the relative yield and cutoff for high energy photons from

radiative muon capture, we cannot state whether or not the process $\mu^- + Z \rightarrow e^+ + Z-2$ has been detected.

However, we can set an upper limit on the branching ratio relative to ordinary muon capture by assuming the validity of the event in question and taking into consideration the expected background. Using the Poisson formula, we have for the probability of R being the correct branching ratio

$$P_n(R) = \frac{(\varepsilon R + b)^n}{n!} \exp(-[\varepsilon R + b]),$$

where n = 1 is the number of observed events, b = 0.013 is the expected background, and ε is the effective number of trials. For the second run we had

$$\varepsilon_2 = N_\mu \cdot f_1 \cdot f_2 \cdot E_{ff} \cdot (\Delta\omega/4\pi)$$
$$= (1.677 \pm 0.023) \times 10^8,$$

where $N_\mu = 4.665 \times 10^{10}$, $f_1 = 0.862$, $f_2 = 0.92$, $E_{ff} = 0.755 \pm 0.07$, and $\Delta\omega/4\pi = (6.0 \pm 0.6) \times 10^{-3}$. For the first run we had

$$\varepsilon_1 = N_\mu \cdot f_1 \cdot f_2 \cdot E_{ff} \cdot (\Delta\omega/4\pi)$$
$$= (0.215 \pm 0.003) \times 10^8,$$

where $N_\mu = 1.552 \times 10^{10}$, $f_2 = 0.610$, $E_{ff} = 0.38 \pm 0.04$, and $\Delta\omega/4\pi = (6.5 \pm 0.7) \times 10^{-3}$. Then $\varepsilon = \varepsilon_1 + \varepsilon_2 = (1.892 \pm 0.026) \times 10^8$.

Calculating $P_1(R)$, normalized to unity at its maximum

value, we find $P_1(R) = 0.1$ when $R = 2.6 \times 10^{-8}$. We can thus say

$$R \leq 2.6 \times 10^{-8}$$

at a 90% confidence level. Then, from Equation (10), we have for the ratio of the coupling constants

$$(G_\Delta/G_V) \leq 0.10^{+0.05}_{-0.03} .$$

CHAPTER V

CONCLUSIONS

The result of this search indicates that the interaction strength of the proposed $\Delta Q = 2$ current is not of the order of magnitude of the vector current. However, it does not preclude the possibility that the one additive lepton number scheme is the correct one.

From the presence of a single event of original momentum 89.9 ± 3.5 MeV/c that is consistent with Reaction (8), but is perhaps due to radiative muon capture, it is obvious that we were approaching the limit of our experimental sensitivity. However, under the conditions of a substantially more intense muon beam, such as that proposed for one of the "meson factories,"[32] it would be possible to pursue this search further. The use of foil targets under those beam conditions might reduce the background from radiative muon capture enough to make it experimentally feasible to reach a branching ratio sensitivity of 10^{-9} to 10^{-10} or to collect a sufficient number of events to determine whether the process exists at the 10^{-8} level.

If the process were not observed at the 10^{-10} level, it would be sufficient to render the one additive lepton number hypothesis inviable. However, as suggested by Pontecorvo,[33] it would still be possible for a $\Delta Q = 2$ current of the type

discussed, but of magnitude 10^{-2} G_V, to be responsible for no neutrino double beta decay (if it exists and lepton conservation fails).

REFERENCES AND FOOTNOTES

[1] See R. E. Marshak, Riazuddin, C. P. Ryan, Theory of Weak Interactions in Particle Physics (Wiley-Interscience, New York, 1969), for a complete discussion of lepton conservation.

[2] This scheme was first suggested by E. J. Konopinski and H. M. Mahmoud, Phys. Rev. 92, 1045 (1953).

[3] B. Pontecorvo, Zh. Eskp. Teor. Fiz 53, 1717 (1967). English translation Soviet Physics JETP 26, 984 (1968).

[4] S. Parker, H. L. Anderson, C. R. Rey, Phys. Rev. 133, B768 (1964).

[5] S. Frankel, et al., Phys. Rev. 130, 351 (1963).

[6] G. Conforto, et al., Nuovo Cimento 26, 261 (1962).

[7] J. J. Amato, et al., Phys. Rev. Letters 21, 1709 (1968).

[8] W. C. Barber, et al., Phys. Rev. Letters 22, 902 (1969).

[9] A. K. Kerman and L. S. Kisslinger, Phys. Rev. 180, 1483 (1969); J. S. Vincent, et al., Phys. Rev. Letters 24, 236 (1970).

[10] H. Arenhovel, M. Danos, H. T. Williams, Nucl. Phys. A162, 12 (1971).

[11] H. Primakoff, Rev. Mod. Phys. 31, 802 (1959).

[12] L. S. Kisslinger, Phys. Rev. Letters 26, 998 (1971).

[13] In the pion core model (see L. S. Kisslinger and H. Feshback, Annals of Physics, to be published), the $\Delta(1236)$ is assumed to be composed of a pion and a core particle. If the interaction here is with the pion, then

$$H^{\Delta Q=2} = \frac{G_\Delta \bar{u}_e (1 - \gamma_5) \gamma_\lambda u_\mu \langle \pi' | (p' + p)_\lambda | \pi \rangle}{\sqrt{4 p_0 p_0'}}$$

, where p and p' are the four-momenta of the π and π' states. This reduces to Equation (9) for the case of a non-relativistic muon.

[14] S. Jena and L.S. Kisslinger, to be published.

[15]Handbook of Chemistry and Physics, R. E. Weast (Ed.), (The Chemical Rubber Co., Cleveland, 1967).

[16]H. Verheul, Nuclear Data Sheets for A = 63, Nuclear Data B2-3-31 (1967); S. C. Pancholi, K. Way, Nuclear Data Sheets for A = 65, Nuclear Data B2-6-1 (1968).

[17]S. E. Sobottka and E. L. Wills, Phys. Rev. Letters 20, 596 (1968).

[18]J. C. Sens, Phys. Rev. 113, 679 (1959).

[19]Science Accessories Corp., Southport, Conn., Model 002a.

[20]The amplifier and discriminator used here were constructed according to designs similar to those described in Lawrence Radiation Laboratory Report UCID 2750.

[21]The scaler assembly and scanning system used was Model 029, Multiple Input Data Acquisition System (MIDAS), Science Accessories Corp., Southport, Conn.

[22]B. Rossi, High Energy Particles (Prentice Hall Inc., Englewood Cliffs, 1952).

[23]B. Zacharov, Nuclear Instruments and Methods 33, 136 (1964).

[24]E. DiCapua, et al., Phys. Rev. 133, B1333 (1964).

[25]M. J. Berger and S. M. Seltzer, Tables of Energy Losses and Ranges of Electrons and Positrons, NASA SP-3012 (1964).

[26]W. T. Chu, I. Nadlehaft, J. Ashkin, Phys. Rev. 137, B352 (1965).

[27]H. P. C. Rood and H. A. Tolhoek, Nucl. Phys. 70, 658 (1965).

[28]L. DiLella, I. Hammerman, L. M. Rosenstein, Phys. Rev. Letters 27, 830 (1971).

[29]L. L. Foldy and J. D. Waleka, Nuovo Cimento 34, 1026 (1964).

[30]J. D. Waleka, Proceedings of the Williamsburg Conference on Intermediate Energy Physics (College of William and Mary, Williamsburg, 1966).

[31]H. W. Fearing, Phys. Rev. 146, 723 (1966).

[32]The "meson factories" now under construction (the Los Alamos Meson Physics Facility [LAMPF] in Los Alamos, New Mexico, the Tri-University Meson Facility [TRIUMF] in Vancouver, British Columbia, the Swiss Institute for Nuclear Research [SIN], and the Joint Institute for Nuclear Research in Dubna, USSR) are expected to produce beams of intensities 10^2-10^3 greater than are now available.

[33]B. Pontecorvo, Phys. Letters 26B, 630 (1968).

The vita has been removed from the scanned document

A SEARCH FOR THE REACTION

$\mu^- + Cu \rightarrow e^+ + Co$

by

Douglas Andrew Bryman

(ABSTRACT)

A search has been performed for the reaction $\mu^- + Cu \rightarrow e^+ + Co$, which is allowed by the lepton conservation scheme that assigns the same lepton number to the μ^-, e^+, ν_μ, and $\bar{\nu}_e$. Momentum analysis of particles emitted following muon capture was performed using a magnetic spectrometer with magnetostrictive readout wire spark chambers. The time of flight through the spectrometer and energy loss in a scintillation counter were measured for each event. One event was observed, at momentum 89.9 ± 3.5 MeV/c, which is consistent with the above process. Background from radiative muon capture was expected to produce ≈ 0.01 events that could simulate the searched for reaction. However, there exists uncertainty in the relative yield and cutoff for high energy photons from radiative muon capture. Although we cannot be certain whether or not the reaction $\mu^- + Cu \rightarrow e^+ + Co$ has been detected, we can set an upper limit on the branching ratio relative to ordinary muon capture of $R \leq 2.6 \times 10^{-8}$

(90% confidence level). According to a calculation by Kisslinger, this can be related to an upper limit on the coupling constant of this type of interaction relative to the vector coupling constant of $(G_{\Delta} / G_{V}) \leq 0.10^{+0.05}_{-0.03}$.